Journal of Molecular Structure 1081 (2015) 506–518

Contents lists available at ScienceDirect

Journal of Molecular Structure

journal homepage: www.elsevier.com/locate/molstruc

FT-IR, FT-Raman, dispersive Raman, NMR spectroscopic studies and NBO analysis of 2-Bromo-1H-Benzimidazol by density functional method

E.B. Sas [a], M. Kurt [a], M. Karabacak [b], A. Poiyamozhi [c], N. Sundaraganesan [d,*]

[a] Department of Physics, Ahi Evran University, Kırsehir, Turkey
[b] Department of Mechatronics Engineering, H.F.T. Technology Faculty, Celal Bayar University, Turgutlu, Manisa, Turkey
[c] Department of Physics, Government Arts College, Dharmapuri 636 705, India
[d] Department of Physics (Engg.), Annamalai University, Annamalai Nagar, 608 002 Chidambaram, Tamil Nadu, India

HIGHLIGHTS

- The vibrational frequencies were calculated by DFT method.
- FTIR and FT-Raman spectra of 2Br1HB were recorded.
- NMR and UV–Vis spectra were also recorded and compared with calculated ones.
- Molecular orbital contributions were studied by TDOS, PDOS and OPDOS.

GRAPHICAL ABSTRACT

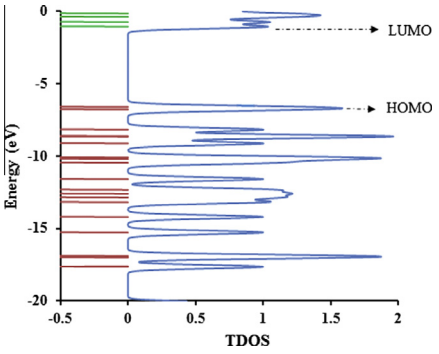

ARTICLE INFO

Article history:
Received 22 June 2014
Received in revised form 11 October 2014
Accepted 13 October 2014
Available online 18 October 2014

Keywords:
2-Bromo-1H-Benzimidazol
FT-IR
FT-Raman and dispersive Raman spectra
NMR
NBO
HOMO–LUMO

ABSTRACT

In this study, geometrical optimization, FT-IR (4000–400 cm^{-1}), FT-Raman (4000–40 cm^{-1}), dispersive Raman (4000–40 cm^{-1}) spectroscopic analysis, electronic structure and ^{1}H and ^{13}C nuclear magnetic resonance (NMR) studies of 2-Bromo-1H-Benzimidazol (abbreviated as 2Br1HB) were undertaken by utilizing DFT/B3LYP with 6-311+G(d,p) basis set. The results of the calculations were applied to simulate spectra of the title compound, which show good agreement with observed spectra. Complete vibrational assignments, analysis and correlations of the fundamental modes for 2Br1HB compound were carried out. Stability of the molecule arising from hyperconjugative interactions, charge delocalization was analyzed using natural bond orbital (NBO) analysis. The molecule orbital contributions were studied by using the total density of states (TDOS), partial density of states (PDOS), and overlap population density of states (OPDOS). The electronic properties like HOMO–LUMO energies and molecular electrostatic potential (MEP) analysis were reported. The calculated HOMO and LUMO energies shows that charge transfer interactions take place within the molecule. Mulliken population analysis on atomic charges was also calculated. Good correlation between the experimental ^{1}H and ^{13}C NMR chemical shifts in DMSO solution and calculated gauge-including atomic orbital (GIAO) shielding tensors were found.

Introduction

Vibrational (IR, Raman) and NMR spectroscopy are extensively used in order to investigate dynamical and structural properties of molecules. With the recent developments in computational

* Corresponding author. Tel.: +91 9442068405.
E-mail address: sundaraganesan_n@yahoo.com (N. Sundaraganesan).

http://dx.doi.org/10.1016/j.molstruc.2014.10.025
0022-2860/

methods, it is possible to describe molecular properties of molecules with close chemical accuracy using theoretical methods [1,2]. Benzimidazole and its derivatives can be used as ligand in the field of coordination chemistry. Benzimidazole moiety is structurally related to Purina bases, and is found in a variety of naturally occurring compounds such as vitamin B12, especially, with the different biological effects such as immunotropic, diuretic, antihistaminic and highly selective p38α MAP inhibition properties [3,4]. Benzimidazole nucleus is a crucial pharmacophore in drug discovery. Pharmaceutical properties including antitumor [5], anti-HIV [6], anti-Parkinson [7] anti-microbial [8] and anti-HCV NS3/NS4A serine protease [9] are unique characteristics known for benzimidazole derivatives. Metal complexes containing benzimidazole based ligand are subject of intensive researches not only owing to their rich coordination chemistry, but also due to a number of established and potential application areas e.g. production of efficient orange light emitting devices (OLEDs), with enhanced stability and efficiency. Benzothiazole and its derivatives are heterocyclic chemicals that contain a benzene ring fused with a thiazole ring. Thiazoles are one of the most rigorously investigated classes of aromatic five membered heterocycles. Halogenated benzimidazoles have raised special interest because of their diversified biological activity. Our title compound is one of the halogenated benzimidazoles; the bromine halogen is attached to the imidazole ring. It has the following Molecular Formula: $C_7H_5BrN_2$; Molecular Weight: 197.03 g/mol and Melting point/range; 191–196 °C.

Recently, Miranda et al. [10] reported bis-(1H-Benzimidazol-2-yl)-methanone: new preparation method, crystal structure, and vibrational spectroscopy and DFT calculations. Abdel-Ghani et al. [11] analyzed novel Ni (II) and Zn (II) complexes coordinated by 2-arylaminomethyl-1H-benzimidazole: molecular structures, spectral, DFT studies and evaluation of biological activity. Sudha et al. [12] investigated molecular structure, vibrational spectroscopic, first-order hyperpolarizability and HOMO, LUMO studies of 2-aminobenzimidazole. Sinha et al. [13] reported quantum-chemical (DFT, MP2) and spectroscopic studies (FT-IR and UV) of monomeric and dimeric structures of 2(3H)-Benzothiazolone. Molecular structure, vibrational, UV and NBO analysis of 4-chloro-7-nitrobenzofurazan by DFT calculations are investigated by Kurt et al. [14].

With the aid of above seen literature, it is clear that there is no quantum mechanical study on the title molecule which has motivated us to undertake a detailed quantum mechanical analysis for understanding the vibrational modes, chemical shifts, HOMO–LUMO, MEP, NMR spectral analysis and thermodynamic properties of the title compound. Therefore, the aim of this study is to fully determine the molecular structure, vibrational modes and wavenumbers by using quantum chemical calculations. Detailed interpretations of the vibrational spectra of our compound have been made based on the calculated potential energy distribution (PED). Besides these calculations, the group contributions of the molecular orbitals and foundation of TDOS (or DOS), PDOS and OPDOS spectra and the contribution of the group to a molecular orbital were calculated using Mulliken population analysis.

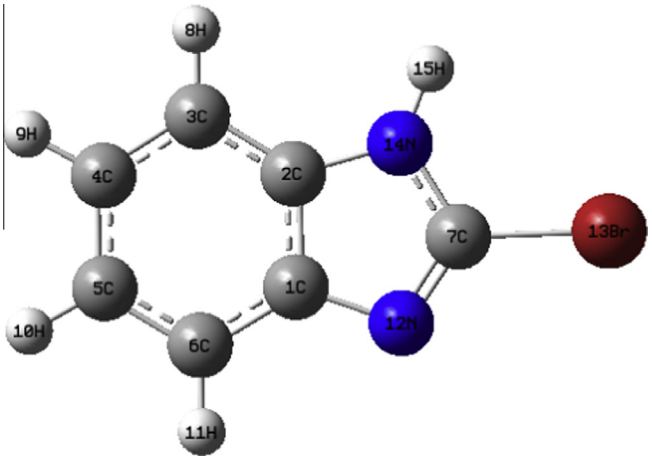

Fig. 1. The theoretical geometric structures of 2Br1HB.

Experimental details

The sample was purchased from Sigma–Aldrich Company with a stated purity of 98%, and it was used as such without further purification. The FT-IR spectrum of the compound was recorded in the region 4000–400 cm^{-1} on a Perkin Elmer FT-IR System Spectrum BX spectrometer calibrated using polystyrene bands. The sample was prepared using a KBr disc technique because of solid state. The spectrum was recorded at room temperature, with a scanning speed of 10 cm^{-1} min^{-1} and the spectral resolution of 4.0 cm^{-1}. FT-Raman spectrum was recorded using 1064 nm line of Nd: YAG laser as excitation wave length in the region 4000–40 cm^{-1} on a Bruker RFS 100/S FT-Raman. The detector is a liquid nitrogen cooled Ge detector. Five hundred scans were accumulated at 4 cm^{-1} resolution using a laser power of 100 mW. The Raman spectrum of the compound was recorded between 4000–40 cm^{-1} with a Thermo Fisher Scientific model DXR dispersive Raman instrument using 780 nm laser excitation. The ^1H, ^{13}C and DEPT NMR spectra were recorded in DMSO solution on a Bruker DPX 400 MHz spectrometer using tetramethylsilane (TMS) as an internal reference at 25 °C.

Computational details

The optimized geometry and vibrational frequencies of 2Br1HB were calculated at the B3LYP/6-311+G(d,p) level with the Gaussian09 program [15]. The molecular structure optimization and corresponding vibrational harmonic frequencies of 2Br1HB were calculated using DFT calculations [16] with the Becke's three-parameter hybrid functional (B3) [17] for the exchange part and the Lee–Yang–Parr (LYP) correlation function [18], for the computation of molecular structure, vibrational frequencies and energies of optimized structures by using Gaussian09 suite of quantum chemical codes. Firstly, the title molecule was optimized, then the optimized structural parameters were used in the vibrational frequencies, isotropic chemical shifts and calculations of electronic properties. The vibrational wavenumber assignments were carried out by combining the results of the Gauss view 5.08 [19] and VEDA4 programs [20]. The calculated IR spectrum, plotted using the pure Lorentzian band shape with a band width of FWHM of 10 cm^{-1} has been compared with the experimental FT-IR spectrum and is found to be well comparable to that of the spectral data obtained by DFT/B3LYP method. The NBO calculations [21] were performed using Gaussian09 [15] package at the same level in order to understand various second order interactions between the filled orbitals of one subsystem and vacant orbitals of another subsystem, which is a measure of the intermolecular delocalization or hyper conjugation. Electronic transitions, vertical excitation energies, absorbance and oscillator strengths were computed with the time-dependent DFT (TD-DFT) method. The electronic properties such as HOMO and LUMO energies were determined by TD-DFT approach. To investigate the reactive sites of the title compound, MEP were evaluated using the B3LYP/6-311+G(d,p) method. The isotropic chemical shifts are frequently used as an aid in identification of organic compounds and accurate

Table 1
Geometrical parameters optimized for 2Br1HB [bond lengths (Å) and bond angles (°)].

Bond lengths	B3LYP	Exp.[a]	Bond lengths	B3LYP	Exp.[a]
C1—C2	1.414	1.400	C4—H9	1.084	0.930
C1—C6	1.397	1.387	C5—C6	1.390	1.374
C1—N12	1.394	1.377	C5—H10	1.084	0.930
C2—C3	1.393	1.386	C6—H11	1.083	0.930
C2—N14	1.388	1.395	C7—N12	1.294	1.338
C3—C4	1.391	1.368	C7—Br13	1.886	–
C3—H8	1.084	0.930	C7—N14	1.374	1.352
C4—C5	1.407	1.392	N14—H15	1.007	0.860
Bond angles (°)	**B3LYP**	**Exp.[a]**	**Bond angles (°)**	**B3LYP**	**Exp.[a]**
C2—C1—C6	119.9	121.3	C4—C5—H10	119.1	119.3
C2—C1—N12	110.4	107.2	C6—C5—H10	119.5	119.3
C6—C1—N12	129.7	131.5	C1—C6—C5	117.8	117.3
C1—C2—C3	122.6	120.6	C1—C6—H11	120.4	121.4
C1—C2—N14	104.5	108.1	C5—C6—H11	121.8	121.4
C3—C2—N14	132.9	131.2	N12—C7—Br13	125.4	–
C2—C3—C4	116.6	117.8	N12—C7—N14	114.7	112.7
C2—C3—H8	122.1	121.1	Br13—C7—N14	119.9	–
C4—C3—H8	121.3	121.1	C1—N12—C7	104.4	107.0
C3—C4—C5	121.6	121.7	C2—N14—C7	106.1	105.1
C3—C4—H9	119.1	119.2	C2—N14—H15	127.9	126.5
C5—C4—H9	119.3	119.2	C7—N14—H15	126.0	126.5
C4—C5—C6	121.5	121.4			
Dihedral angles (°)	**B3LYP**	**Exp.[a]**	**Dihedral angles (°)**	**B3LYP**	**Exp.[a]**
C6—C1—C2—C3	0.0	0.8	C2—C3—C4—C5	0.0	0.4
C6—C1—C2—N14	180.0	177.7	C2—C3—C4—H9	180.0	–
N12—C1—C2—C3	−180.0	−176.2	H8—C3—C4—C5	−180.0	–
N12—C1—C2—N14	0.0	0.8	H8—C3—C4—H9	0.0	–
C2—C1—C6—C5	0.0	−1.0	C3—C4—C5—C6	0.0	0.8
C2—C1—C6—H11	180.0	–	C3—C4—C5—H10	180.0	–
N12—C1—C6—C5	180.0	175.1	H9—C4—C5—C6	−180.0	–
N12—C1—C6—H11	0.0	–	H9—C4—C5—H10	0.0	
C2—C1—N12—C7	0.0	−0.1	C4—C5—C6—C1	0.0	0.8
C6—C1—N12—C7	180.0	−176.6	C4—C5—C6—H11	−180.0	–
C1—C2—C3—C4	0.0	−0.5	H10—C5—C6—C1	−180.0	–
C1—C2—C3—H8	180.0	–	H10—C5—C6—H11	0.0	–
N14—C2—C3—C4	−180.0	−176.6	Br13—C7—N12—C1	180.0	–
N14—C2—C3—H8	0.0	–	N14—C7—N12—C1	0.0	−0.7
C1—C2—N14—C7	0.0	−1.2	N12—C7—N14—C2	0.0	1.2
C1—C2—N14—H15	−180.0	–	N12—C7—N14—H15	180.0	–
C3—C2—N14—C7	−180.0	−175.3	Br13—C7—N14—C2	180.0	–
C3—C2—N14—H15	0.0	–	Br13—C7—N14—H15	0.0	–

[a] Taken from Ref. [28].

predictions of molecular geometries are essential for reliable studies of magnetic properties. The ^{13}C and ^{1}H NMR isotropic shieldings were calculated with the GIAO method [22,23], using the optimized parameters obtained from B3LYP/6-311+G(d,p) method. The GIAO method is one of the most common approaches for calculating nuclear magnetic shielding tensors. Besides these calculations, the group contributions of the molecular orbitals and preparation of TDOS (or DOS), PDOS and OPDOS spectra Gauss Sum 2.2 [24] were used. The contribution of the group to a molecular orbital was calculated using Mulliken population analysis. The PDOS and OPDOS spectra were created by convoluting the molecular orbital information with Gaussian curves of unit height and a FWHM (Full Width at Half Maximum) of 0.3 eV. The changes in the thermodynamic functions (the heat capacity, entropy, and enthalpy) were investigated for the different temperatures from the vibrational frequency calculations of 2Br1HB molecule.

Prediction of Raman intensities

The Raman activities (S_i) calculated by Gaussian 09 program [15] have been converted to relative Raman intensities (I^{Ra}). The theoretical Raman intensity (I^{Ra}), which simulates the measured Raman spectrum, is given by the equation [25,26]:

$$I_i^{Ra} = C(v_0 - v_i)^4 v_i^{-1} B_i^{-1} S_i \quad (1)$$

where B_i is a temperature factor which accounts for the intensity contribution of excited vibrational states, and is represented by the Boltzman distribution:

$$B_i = 1 - (\exp \_hv_i c/kT) \quad (2)$$

In Eq. (1) v_0 is the frequency of the laser excitation line (in this work, we have used the excitation frequency $v_0 = 9398.5\ cm^{-1}$, which corresponds to the wavelength of 1064 nm of a Nd:YAG laser), v_i is the frequency of normal mode (cm^{-1}), while S_i is the Raman scattering activity of the normal mode Q_i. I_i^{Ra} is given in arbitrary units (C is a constant equal 10^{-12}). In Eq. (2) h, k, c, and T are Planck and Boltzman constants, speed of light and temperature in Kelvin, respectively. Thus, the presented theoretical Raman intensities have been computed assuming B_i equal 1. The theoretical Raman spectrum has been calculated by the Raint program [27]. The simulated spectrum was plotted using a Lorentzian band shape with a half-width at half-height (HWHH) of 10 cm^{-1}.

Results and discussion

Optimized geometry

A view of the molecular structure of the compound 2Br1HB is shown in Fig. 1. The calculated bond lengths, bond angles and dihedral angles with DFT/B3LYP with 6-311+G(d,p) basis set are given

Table 2
Comparison of the calculated and experimental vibrational wavenumbers (cm^{-1}) and proposal assignments of 2Br1HB.

	Experimental wavenumbers			Theoretical wavenumbers				PED (10%)
No.	FT-IR	FT-Raman	Dispersive Raman	Scaled	[a]I_{IR}	[b]S_{Ra}	[c]I_{Ra}	Assignments[d]
A′				3546	82.57	88.67	0.08	υNH(100)
A′				3101	7.89	228.63	0.3	υCH(99)
A′				3092	15.09	144.36	0.19	υCH(100)
A′				3081	8.68	116.13	0.15	υCH(99)
A′	3049vw	3070s	3070s	3071	0.32	49.36	0.07	υCH(100)
A′		1600m	1599m	1607	14.46	14.75	0.09	υCC(59), υCN(21), δHCC(12)
A′				1572	2.32	23.63	0.15	υCC(24), δCNC(24), δCCC(23), δCCN(15)
A′	1500vw	1500vw		1476	57.5	29.43	0.2	δCCH(31), υCC(30), υCN(18), δHNC(13),
A′				1466	58.73	35.96	0.25	υCN(42), υCC(24), δHCC(19)
A′	1400m	1430s	1430s	1422	86.28	32.27	0.24	δCCH(44), υNC(28), δCCN(15)
A′	1350s	1360m		1370	101.63	32.31	0.25	δHNC(29), υCN(19), δHCC(17), υCC(13)
A′			1339m	1328	61.86	11.03	0.09	υCC(41), δCCH(14), δCNC(11), υCN(10)
A′	1258s	1270vs	1270vs	1269	22.71	8.58	0.08	δCCH(54), υCN(26), υCC(12)
A′		1220s		1239	44.95	101.49	0.93	υCC(38), υCN(31), δHCC(17)
A′	1215vs		1215s	1198	11.75	30.87	0.3	υCN(35), δCCH(23), υCC(16)
A′		1150w	1142m	1137	1.84	4.51	0.05	δCCH(66), υCC(11)
A′		1120s	1112s	1116	21.56	31.59	0.34	υCN(30), δHNC(30), δHCC(11)
A′				1094	5.22	2.73	0.03	δCCH(46), υCC(18), δCCC(15)
A′		1010s	1010vs	996	2.71	30.73	0.4	δCNC(24), δCCN(23), δHCC(17), υCC(14), δNCN(12)
A″	973s			955	0.02	0.06	0	γCH(80), ΓCCCN(16)
A′				935	20.43	5.14	0.07	δNCN(30), υCN(29), δCCN(20)
A″		920w		916	1.88	0.52	0.01	γCH(73), ΓCNCC(14)
A′		852vw	863vw	874	1.13	0.62	0.01	δCCC(63), υCN(27)
A″	831w			829	0.38	0.44	0.01	γCH(84), ΓCNCC(11)
A′		804m	805m	789	0.91	24.31	0.45	υCC(40), δCCN(22), υCN(16)
A″		739w		737	37.92	0.97	0.02	γCH(47), ΓCNCN(28), ΓCCCN(14), ΓCNCC(10)
A″	717m		717s	724	42.23	0.18	0	γCH(62), ΓCCCN(29)
A″		629s	630m	646	8.56	0.01	0	ΓCCCN(47), ΓHNCN(24), ΓBrNNC(16)
A′	614s			610	0.27	8.13	0.22	δCNC(43), υCC(36)
A′		577w		569	2.86	0.86	0.03	δCCC(35), δCCN(14), δCNC(12), υCBr(10)
A″				566	2.65	0.09	0	ΓCCCN(37), ΓCNCC(31), ΓCNCN(16), ΓHCCC(14)
A′		474vw		458	4.15	0.66	0.03	δCCN(64), δBrCN(22)
A″				421	18.87	0.08	0	ΓCCCN(64), ΓHCCC(22)
A″				400	68.81	0.49	0.02	ΓHNCN(67), ΓCNCN(22)
A″			303s	289	0.53	0.48	0.04	ΓCCCN(60), ΓBrNNC(35)
A′				287	3.44	8.06	0.66	υCBr(68), υCN(12)
A″				244	2.34	0.24	0.03	ΓCCCN(55), ΓCNCN(39)
A′			138s	176	0.37	0.18	0.03	δBrCN(70), δCCN(16)
A″				96	1.09	1.84	1	ΓBrNNC(41), ΓCCCN(38), ΓCNCN(18)

[a] I_{IR} – IR intensity in km/mol.
[b] S_i – Raman scattering activity in Å/amu.
[c] I_{Ra} – Raman intensity in arb units.
[d] υ; stretching, δ; in plane bending, γ; out of plane bending, Γ; torsion.

in Table 1. The keen literary survey reveals that the experimental data on the geometric structure of the title compound are not available till now. Due to the absence of experimental data, our optimized structural parameters are compared with similar systems for which the crystal structures have been solved. The optimized structure of 2Br1HB and experimental structure of closely related molecule 2-[4-(1H-1,2,4-Triazol-1-yl)phenyl]-1Hbenzimidazole available in the literature [28] were compared. The calculated geometrical parameters represent a good agreement with experimental values. The C—C bond lengths in the benzene ring vary in the range of 1.390–1.407 Å by DFT method, 1.368–1.392 Å by XRD, except C1—C2 at the largest 1.414 Å value by DFT method, 1.400 Å by XRD which is due to the fusion of heterocyclic ring. From Table 1, it is clear that some of the bond lengths and bond angles are found to be greater than experimental data. This overestimation can be explained that the theoretical calculations are performed in gaseous phase while the experimental methods are performed in solid phase. It is well known that due to a change in the charge distribution on the carbon atoms of benzene ring changes the C—H bond lengths belong to substitution. The C—H bond lengths are found constant, at 1.084 Å by DFT method, 0.930 Å by XRD. The C7—N14 bond length (1.374 Å by DFT method) is shorter than the other C—N (C1—N12 = 1.394 Å and C2—N14 = 1.388 Å by DFT method) bond lengths, and a noticeable difference between the calculated and experimental data is observed. It may be due to the presence of intermolecular hydrogen bonding [29]. In the molecular structure, intermolecular N—H···N hydrogen bond link, the bond length of N14—H15 = 1.007 Å by DFT method and from experimental value it is 0.860 Å. The C—Br bond length is calculated at 1.886 Å by B3LYP method, which gives slightly less than the literature values of 1.924 Å [30] and 1.921 Å [31] respectively. The C2—C3—C4 and C1—C6—C5 bond angles both involving a common carbon atom of the two fused rings are reduced at 116.6° and 117.8°, while all other C—C—C bond angles of the benzene ring are above 120° (C3—C4—C5 = 121.6° and C4—C5—C6 = 121.5° see Table 1). The optimized bond angles of the imidazole ring are in good agreement with experimental values. For example C3—C2—N14 angle is calculated at 132.9°, which is observed at 131.2°. The dihedral angle between the benzene ring and imidazole ring C6—C1—C2—N14 = 180°, N14—C2—C3—C4 = −180° and N12—C1—C2—C3 = −180° shows good agreement with experimental values at 177.7°, −176.6° and −176.2° respectively.

Vibrational assignments

The experimental and computed vibrational wavenumbers, their IR intensities and the detailed description of normal modes

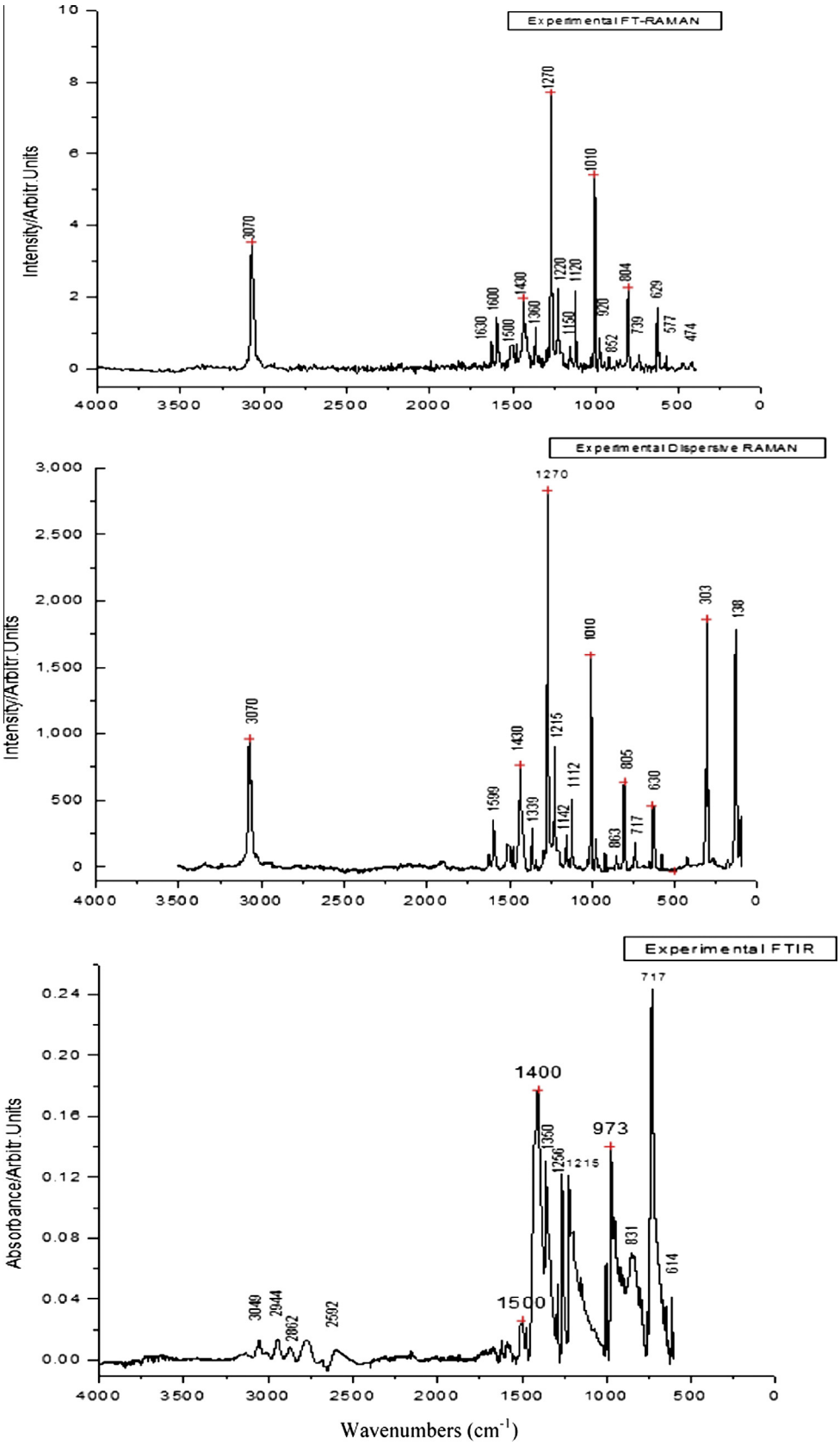

Fig. 2. The experimental FT-IR, FT-Raman and dispersive Raman spectra of 2Br1HB.

of vibration of 2Br1HB, carried out in terms of their contribution to the potential energy, are given in Table 2. The experimental FT-IR, FT-Raman, dispersive Raman spectra and the calculated (with the scale factor) infrared and Raman spectra of the compound 2Br1HB are shown in Figs. 2 and 3 respectively. DFT vibrational unscaled wavenumbers are known to be higher than the experimental

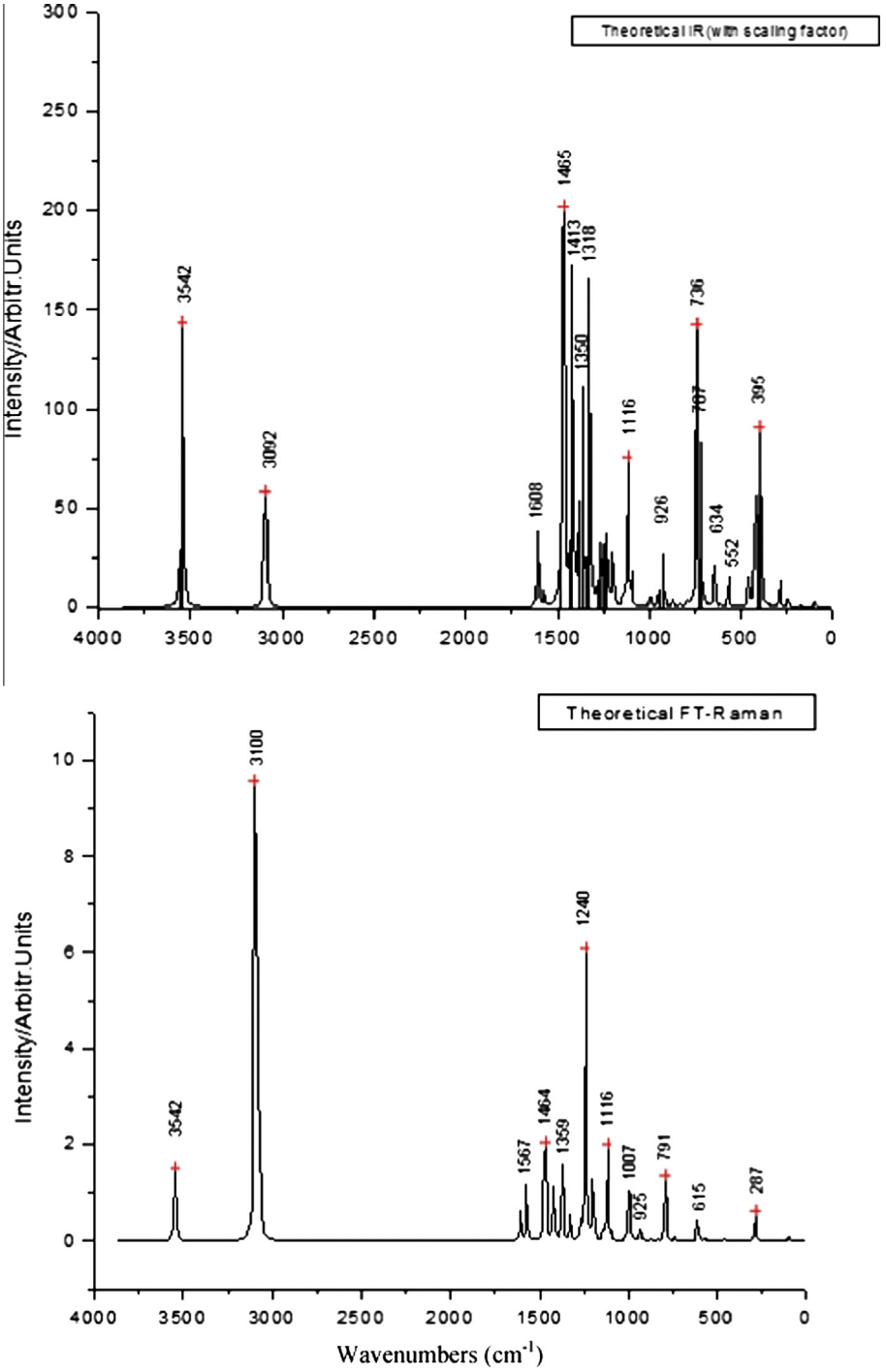

Fig. 3. The calculated (with the scale factor) infrared and Raman spectra of 2Br1HB.

wavenumbers partly because of the neglect of anharmonicity, and partly because of the approximate nature of the quantum mechanical methods, they were scaled down by a uniform scaling factor of 0.9688 [32] and the scaled wavenumbers in general show good agreement with the experimental ones. The 2Br1HB molecule has 15 atoms, which possess 39 normal modes of vibrations, which are distributed by symmetry species as: $\Gamma vib = 27\ A' + 12\ A''$. In agreement with C_S point group symmetry. All vibrations are active both in Raman and infrared spectra. The PED for each normal mode among the symmetry coordinates of the molecules was calculated. In order to investigate the performance and vibrational wavenumbers of the title compound root mean square value (RMS) and correlation coefficient between calculated and observed wavenumbers were calculated Fig. 4. RMS values of wavenumbers were evaluated using the following expression [33]:

$$\sqrt{\frac{1}{n-1}\sum_{i}^{n}\left(\upsilon_i^{calc}-\upsilon_n^{exp}\right)^2} \tag{3}$$

where n is the number of the experimental or calculated data. The RMS errors of the observed IR and Raman bands are found to be 9.22 and 11.97 respectively. Correlation graph between the calculated and experimental frequencies of infrared and Raman for 2Br1HB molecule is shown in Fig. S1.

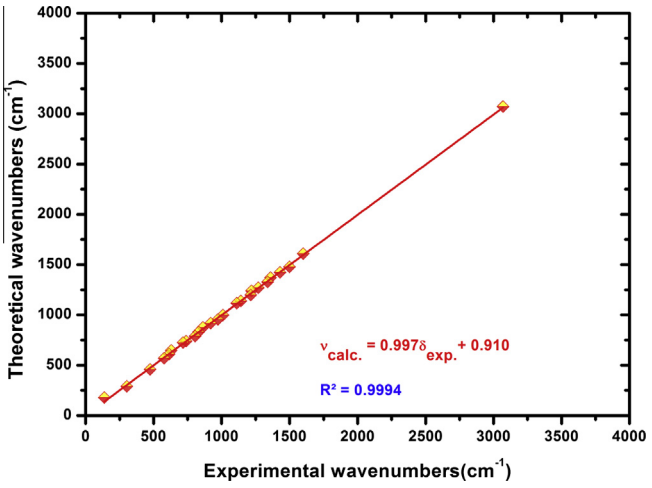

Fig. 4. Correlation graphic of the calculated and experimental frequencies of 2Br1HB.

C—H vibrations

The aromatic C—H stretching vibrations are normally found between 3100–3000 cm^{-1} [34,35]. In this region the bands are not affected appreciably by the nature of substituents. All the aromatic C—H stretching bands are found to be weak and this is due to decrease of dipole moment caused by reduction of the negative charge on the carbon atom. This reduction occurs because of the electron withdrawal from the carbon atom by substituent due to the decrease of inductive effect, which in turn by the increase in chain length of the substituent [36]. In the present study the bands observed at 3049 cm^{-1} in FT-IR and at 3070 cm^{-1} in FT-Raman and dispersive Raman spectra are assigned to the C—H stretching vibrations. The computed wavenumbers at 3101, 3092, 3081 and 3071 cm^{-1} by B3LYP method are identified as C—H stretching modes with A′ symmetry. The PED contribution of the aromatic C—H stretching modes indicates that these are also highly pure modes. The C—H in-plane bending vibration is usually expected to occur in the region 1300–1000 cm^{-1} and these vibrations are very useful for characterization purpose [37,38]. The C—H in-plane bending vibrations of benzimidazole are coupled with ring C—C and C═N stretching modes as evident from PED column of Table 2. In our title molecule the C—H in-plane bending vibrations are observed at 1400, 1258 and 1215 cm^{-1} in FT-IR and at 1430, 1270 and 1150 cm^{-1} in FT-Raman and at 1430, 1270, 1215 and 1142 cm^{-1} in dispersive Raman spectra are assigned as C—H in-plane bending vibrations. Theoretically predicted wavenumbers at 1422, 1269, 1198, 1137 and 1094 cm^{-1} by B3LYP method show the C—H in-plane bending vibrations with symmetry of A′. The C—H out-of-plane bending vibrations are strongly coupled vibrations and occur in the region 1000–750 cm^{-1} [39,40]. In this work, the out-of-plane bending vibrations were recorded at 973, 831 and 717 cm^{-1} in FT-IR and at 920 and 739 cm^{-1} in FT-Raman and at 717 cm^{-1} in dispersive Raman spectra. These bands are computed at 955, 916, 829, 737 and 724 cm^{-1} by B3LYP method. It is evident from the PED column that these modes contributed between 47 and 84% with A″ symmetry.

C—C vibrations

The ring stretching C—C vibrations are very much important and highly characteristic of the aromatic ring itself. The C—C stretching vibration modes in the phenyl ring generally occur in the region 1430–1625 cm^{-1}. Varsanyi [41] observed at 1625–1590, 1575–1590, 1470–1540, 1430–1465 and 1280–1380 cm^{-1} from the frequency ranges given by for the five bands in the region,

Table 3
Experimental and calculated chemical shifts (ppm) of 2Br1HB.

Atom	Calculated/ B3LYP/6-311G+(d,p)				Exp.
	DMSO	Ethanol	Water	Gas	DMSO
C7	149.56	149.48	149.60	147.67	139.81
C1	148.87	149.01	148.95	149.88	127.25
C2	141.00	140.97	141.01	140.20	127.25
C4	128.56	128.53	128.57	127.78	122.85
C5	126.76	126.76	126.76	126.87	122.85
C6	123.55	123.64	123.51	125.35	114.97
C3	113.93	113.81	113.98	111.29	114.97
H15	8.66	8.64	8.68	7.87	10.67
H11	7.84	7.84	7.84	7.84	7.54
H8	7.65	7.64	7.66	7.30	7.54
H9	7.50	7.49	7.50	7.30	7.20
H10	7.47	7.47	7.48	7.34	7.20

and generally the bands are of variable intensity. In the present study, the wavenumbers observed in FT-IR spectrum at 1500, 1350, 1258 and 1215 cm^{-1}, in FT-Raman spectrum at 1600, 1500, 1360, 1270, 1220 cm^{-1} and in dispersive Raman spectrum at 1599, 1339, 1270 cm^{-1} are assigned to C—C stretching vibrations. The predicted wavenumbers at 1607, 1572, 1476, 1466, 1370, 1328, 1269, 1239, 1198 and 1094 cm^{-1} by B3LYP method identified as C—C stretching vibrations show good agreement with the experimental findings. The C—C—C in plane bending bands always occur between the value 1000–600 cm^{-1} [42]. In our case C—C—C in plane bending bands is observed at 852 & 577 cm^{-1} in FT-Raman and at 863 cm^{-1} in dispersive Raman spectrum. They are calculated at 1094, 874 and 569 cm^{-1} by B3LYP method.

C—N and C═N vibrations

The identifications of C═N and C—N vibrations are a difficult task, since the mixing of several bands is possible in the region. Karabacak et al. [43] assigned C═N and C—N stretching at 1689 and 1302 cm^{-1} in FT-IR spectrum, respectively. Sundaraganesan et al. [44] assigned C—N stretching vibration at 1281 cm^{-1} for benzimidazole. In the present work, C═N stretching vibration is observed at 1600 cm^{-1} in FT-Raman spectrum and computed at 1607 cm^{-1} by B3LYP method. C—N stretching vibrations are computed at 1239–1422 cm^{-1} by B3LYP method, and it is also observed in the range of 1400–1258 cm^{-1} in FT-IR spectrum and in the range of 1430–1220 cm^{-1} in FT-Raman spectrum and 1430–1270 cm^{-1} in dispersive Raman which are correlated well with the experimental data. In addition to these vibrations, the C—N—C, N—C—N and C—C—N bending vibrations (i.e. in plane and out-of-plane) have been assigned by PED, showing good agreement with recorded spectral data.

N—H vibrations

The N—H stretching vibrations generally give rise to bands in the range of 3500–3300 cm^{-1} [45,46]. In the present case, the band observed at 3400vw cm^{-1} (Dispersive Raman) is assigned as NH stretching vibrations. The computed wavenumber at 3546 cm^{-1} by B3LYP method is identified as N—H stretching mode. It is a pure mode evident from the PED column which contributes to 100%. The intermolecular hydrogen bonding is simply revealed in the deviation of theoretical wavenumbers of N—H stretching modes. Panicker et al. [47] reported NH deformation bands at 1538, 1220 cm^{-1} in IR spectrum and at 1538, and 1223 cm^{-1} theoretically. In our work the bands at 1500, 1350 cm^{-1} in FT-IR and at 1500, 1360 &1120 cm^{-1} in FT-Raman spectra are observed as NH in plane bending vibration, which is in well agreement with calculated bands at 1476, 1370 and 1116 cm^{-1} by B3LYP method. The band at 629 cm^{-1} in FT-Raman spectra, 630 cm^{-1} in dispersive Raman and predicted scaled wavenumbers at 646 and 400 cm^{-1} are assigned as NH torsional modes.

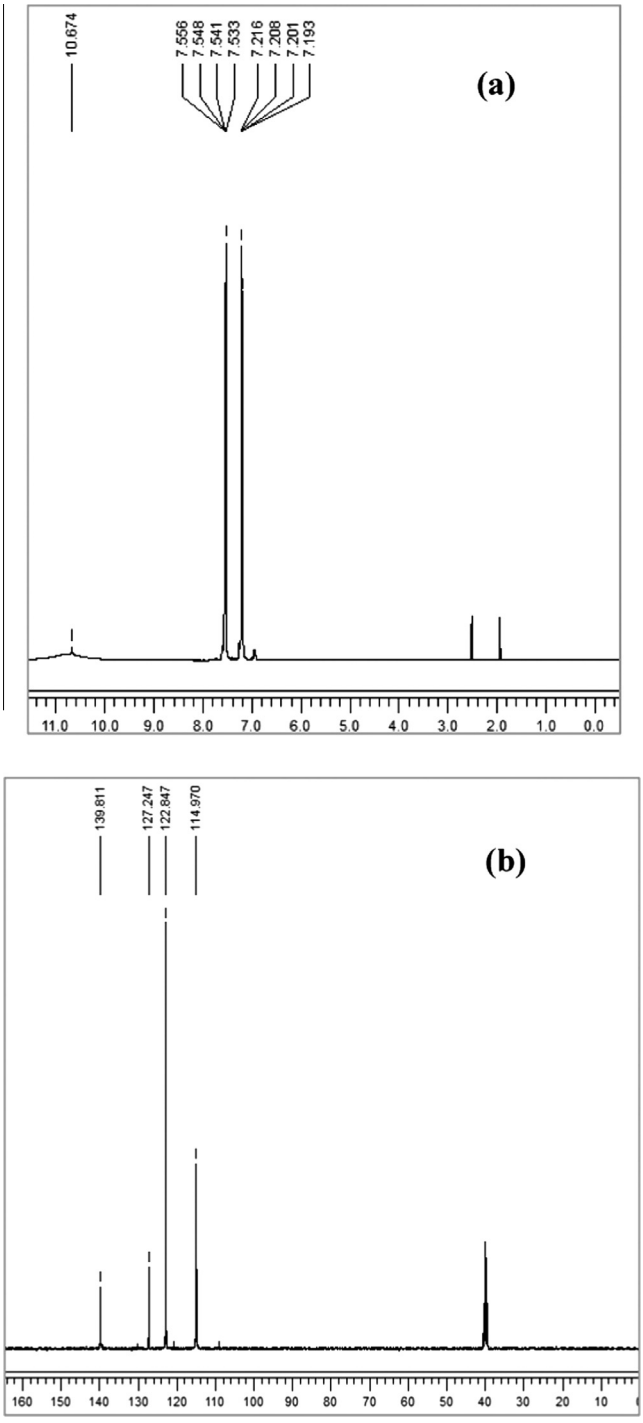

Fig. 5. (a) ^{1}H NMR (b) ^{13}C NMR spectra of 2Br1HB in DMSO solution.

C—Br vibrations

The C—Br stretching mode appears at 480–200 cm^{-1} wavenumber region as reported by Varsanyi [41]. In our present case C—Br stretching mode is observed at 577 cm^{-1} in FT-Raman spectrum and it is also predicted at 569 & 287 cm^{-1} by B3LYP method. The band at 474 cm^{-1} in FT-Raman spectra and theoretically predicted wavenumbers at 458 and 176 cm^{-1} by DFT method are assigned as BrCN in plane bending vibrations. The scaled wavenumbers at 289 and 96 cm^{-1} by DFT method are identified as BrNNC out of plane bending vibrations with A'' symmetry.

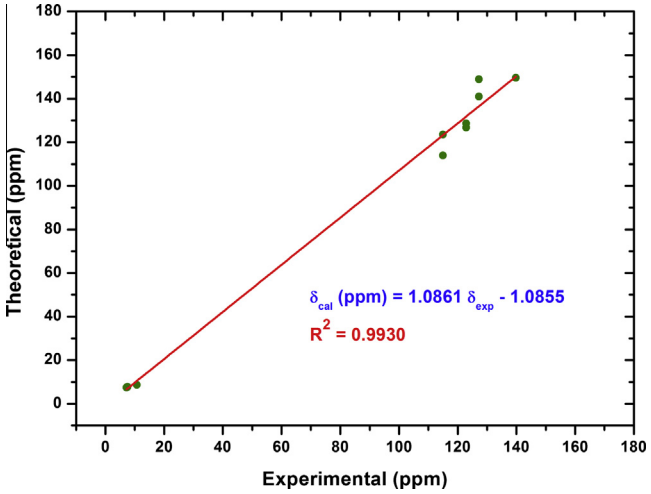

Fig. 6. Correlation graphic of the calculated and experimental (total) chemical shifts of 2Br1HB.

Table 4
Comparison of experimental (in ethanol, DMSO, water and gas phase) and calculated absorption wavelengths (λ, nm), excitation energies (E, eV) and oscillator strength (f) of 2B1HB.

TD-DFT/ B3LYP/6-311+G(d,p)			
λ (nm)	E (eV)	f	Transition
Ethanol			
252.62	4.9079	0.1860	H − 1 → L, H − 1 → L + 2, H → L
243.88	5.0838	0.0003	H → L + 1
239.45	5.1779	0.1501	H → L
DMSO			
252.79	4.9047	0.1951	H − 1 → L, H − 1 → L + 2, H → L
243.73	5.0870	0.0003	H → L + 1
239.63	5.1740	0.1540	H − 1 → L
Water			
252.50	4.9103	0.1821	H − 1 → L, H − 1 → L + 2, H → L
243.61	5.0895	0.0003	H → L + 1
239.32	5.1808	0.1464	H − 1 → L
Gas phase			
251.11	4.9374	0.1141	H − 1 → L, H − 1 → L + 3, H → L
248.35	4.9923	0.0003	H → L + 1
235.01	5.2756	0.0001	H − 1 → L + 1

Natural bond orbital analysis

Natural bond orbital (NBO) analysis is an essential tool for studying intra and intermolecular bonding and interaction among bonds, and also provides a convenient basis for investigating charge transfer or conjugative interaction in molecular systems. Some electron donor orbital, acceptor orbital and the interacting stabilization energy resulting from the second-order micro disturbance theory is reported [48]. The energy values for the interaction between the filled '*i*' and vacant orbital '*j*', calculated by the second order perturbation theory at the B3LYP/6-311+G(d,p) level were tabulated (Table S1). Gaussian 09W software [15] with the NBO 3.1 program [21] was used for analysis of the natural orbitals and their interactions. The result of interaction is a loss of occupancy from the concentrations of electron NBO of the idealized Lewis structure into an empty non-Lewis orbital. For each donor (i) and acceptor (j), the stabilization energy $E^{(2)}$ associates with the delocalization $i \rightarrow j$ which is estimated as.

$$E^{(2)} = \Delta E_{ij} = q_i \frac{F(i,j)^2}{(\varepsilon_j - \varepsilon_i)} \quad (4)$$

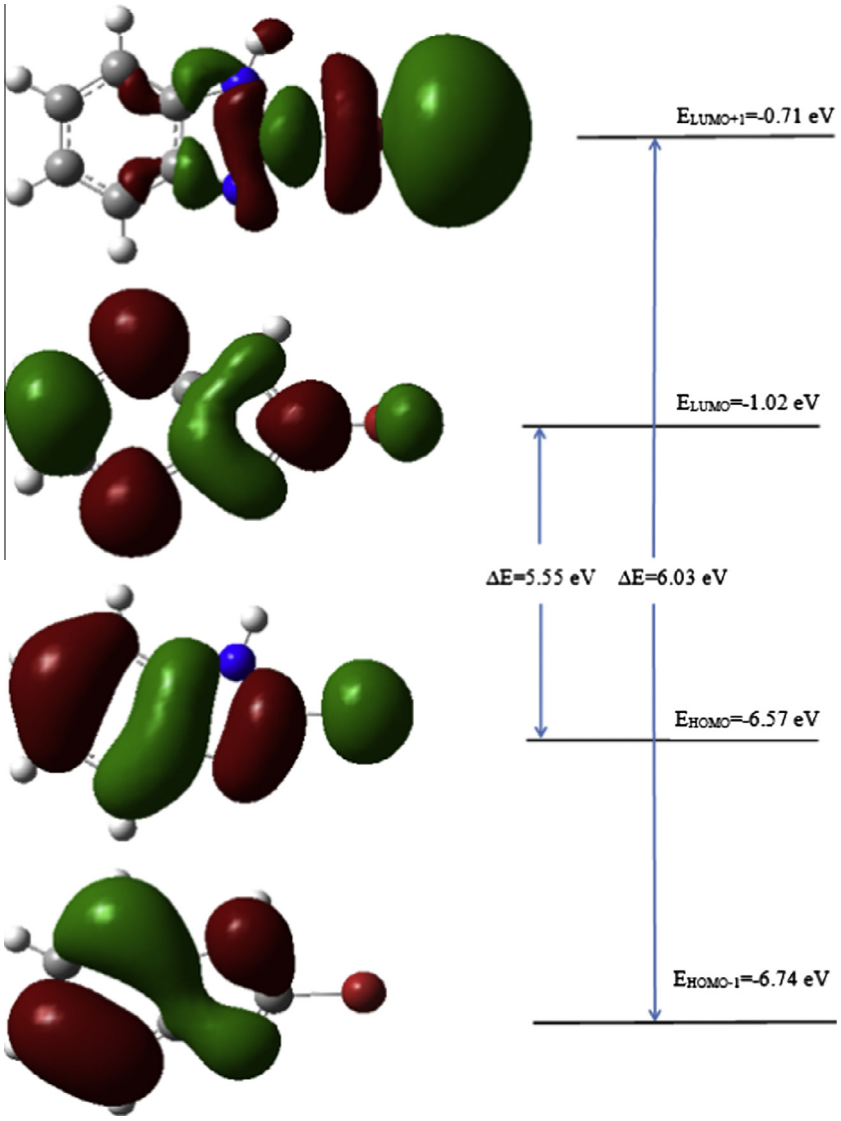

Fig. 7. The frontier molecular orbitals of 2Br1HB for gas phase.

q_i is the donor orbital occupancy; E_i, E_j is the diagonal elements and $F(i,j)$ is the off diagonal NBO Fock matrix element.

In our present study the π(C1—C2) bond is interacting with π*(C3—C4), π*(C5—C6) and π*(C7—N12) with the energies 18.45, 18.31 and 15.30 kJ/mol, respectively. The hyper conjugative interaction between σ(C1—C2) → σ*(C7—Br13) has low stabilization energy 1.74 kJ/mol. The σ electron of (C1—N12) is distributed to σ*(C7—Br13), which leads to delocalization energy 10.78 kJ/mol. The π(C3—C4) bond is contributing energy 20.33 kJ/mol with electron density 1.72 to bond π*(C1—C2). The important interactions in the title molecule having π(C5—C6) and π(C7—N12) with that of anti-bonding (C1—C2) result in the stabilization of 18.91 kJ/mol and 16.11 kJ/mol, respectively. The maximum energy occurs from N14 LP(1) to anti-bonding π*(C1—C2) with delocalization energy

Table 5
The Calculated energy values of 2Br1HB molecules using by the TD-DFT/B3LYP method using 6-311G+(d,p) basis set.

	Gas	DMSO	Water	Ethanol
E_{total} (Hartree)	−2953.49712773	−2953.51703177	−2953.51719473	−2953.51668285
E_{HOMO} (eV)	−6.57	−6.66	−6.66	−6.65
E_{LUMO} (eV)	−1.02	−1.09	−1.09	−1.09
E_{HOMO-1} (eV)	−6.74	−6.78	−6.78	−6.78
E_{LUMO+1} (eV)	−0.71	−0.70	−0.70	−0.70
$E_{HOMO-1-LUMO+1\ gap}$ (eV)	6.03	6.08	6.08	6.08
$E_{HOMO-LUMO\ gap}$ (eV)	5.55	5.57	5.57	5.56
Chemical hardness (h)	2.77	2.78	2.78	2.78
Electronegativity (χ)	3.79	3.87	3.87	3.87
Chemical potential (μ)	−3.79	−3.87	−3.87	−3.87
Electrophilicity index (ω)	2.59	2.69	2.69	2.69

30.99 kJ/mol. The bonding π(C1—C2) of NBO is conjugated with anti-bonding (C5—C6) of NBO which leads to an enormous stabilization energy 196.64 kJ/mol.

^{1}H and ^{13}C NMR analysis

The isotropic chemical shifts are frequently used as an aid in identification of reactive ionic species. It is recognized that accurate predictions of molecular geometries are essential for reliable calculations of magnetic properties. The molecular structure of 2Br1HB is optimized by using B3LYP method with 6-311+G(d,p) as basis set. Then, GIAO ^{13}C and ^{1}H chemical shift calculations of the title compound are made by using B3LYP method in conjunction with the same basis set. The ^{13}C and ^{1}H observed and theoretical chemical shifts, isotropic shielding tensors of 2Br1HB with 6-311+G(d,p) basis set are presented in Table 3. The experimental ^{1}H and ^{13}C NMR spectra of the title compound in DMSO solvent are shown in Fig. 5a and b, respectively. The correlation between the experimental and calculated chemical shifts (total) obtained by DFT/B3LYP method is shown in Fig. 6. The aromatic carbons give signals in the overlapped areas of the spectrum with chemical shift values from 100 ppm to 150 ppm [49]. In our case the ^{13}C NMR chemical shift, the observed signal at 139.81 ppm is assigned to the C7 carbon of the imidazole ring, which is bonded to the Br atom. Due to this Br substitution on the carbon atom C7, its chemical shift value is high when compared with other carbon atoms. This is also calculated at 149.56, 149.48, 149.60, and 147.67 ppm by B3LYP method in DMSO, ethanol, water, and gas phase, respectively. The C1 and C2 belonging to imidazole ring appeared as doublet, which is observed at 127.25 ppm and calculated at 148.87 for C1 and 141.0 for C2 by B3LYP method in DMSO. Similarly C4 and C5 carbon atoms of the phenyl ring appeared as doublet, which is also observed 122.85 ppm in DMSO and it is also calculated at 128.56 ppm for C4 and 126.76 ppm for C5 in DMSO by B3LYP method. Other doublet peaks are observed in DMSO for C3 and C6 atoms, and the value of the chemical shift for above said carbons is 114.97 ppm. This is in good agreement with calculated chemical shifts at 113.93, 113.81, 113.98 and 111.29 ppm for C3 atom and at 123.55, 123.64, 123.51 and 123.35 ppm for C6 atom in DMSO, ethanol, water, and gas phase, respectively. In the ^{1}H NMR spectrum of the title compound, H15 proton appears as a singlet. This proton shift is observed at 10.67 ppm in DMSO and calculated at 8.66, 8.64, 8.68, 7.87 ppm by DFT method in DMSO, ethanol, water, gas phase, respectively. This proton shift is the highest shift when compared with other proton shifts. The reason for this may be due to intermolecular interaction (N—H···N) between the NH proton and N atom of the imidazole. The H8 & H11, H9 & H10 protons of the phenyl ring appeared as doublet; this is observed at 7.54 ppm (H8 & H11) and 7.20 ppm (H9 & H10) in DMSO solvent and it is also calculated at 7.65 (H8), 7.84 ppm (H11), 7.50 ppm (H9) and 7.47 ppm (H10) by B3LYP method in DMSO solvent. The entire experimental chemical shift values are in good agreement with the calculated chemical shift values by DFT method in DMSO. Correlation graph between the calculated and experimental chemical shifts of proton NMR and carbon NMR for 2Br1HB molecule is shown in Fig. S2.

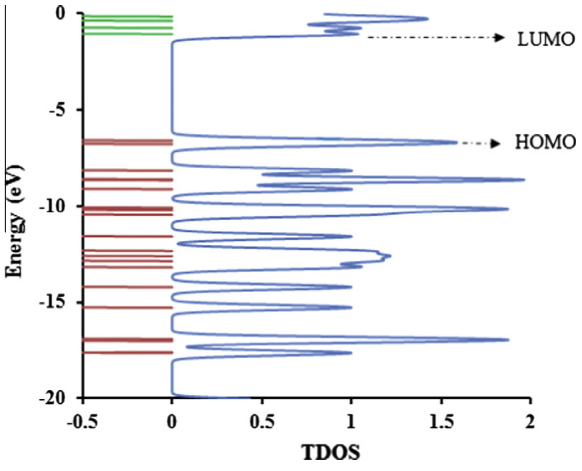

Fig. 8. The TDOS diagram of 2Br1HB.

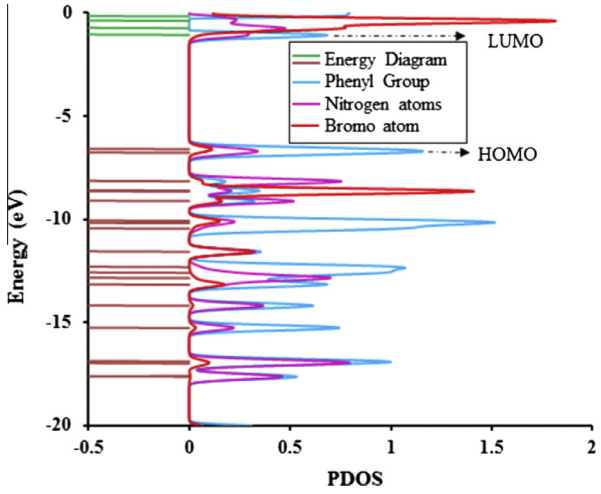

Fig. 9. The PDOS diagram of 2Br1HB.

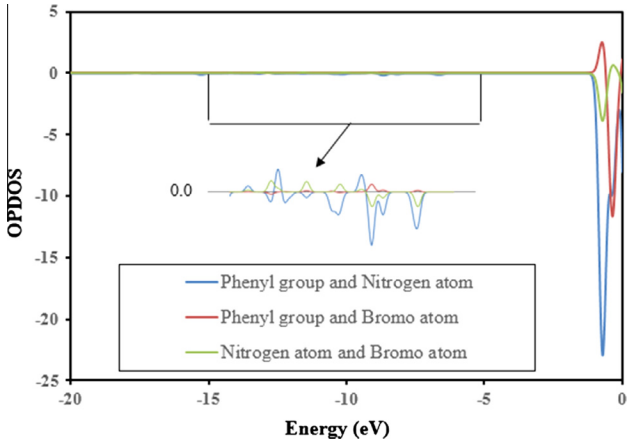

Fig. 10. The OPDOS diagram of 2Br1HB.

Electronic properties

UV–Vis spectral analysis

Ultraviolet spectra analyses of 2Br1HB were investigated in gas phase and in three different solvents (ethanol, DMSO and water) by theoretical calculation. On the basis of fully optimized ground-state structure, TD-DFT/B3LYP/6-311+G(d,p) calculations were used to determine the low-lying excited states of 2Br1HB. The theoretical absorption wavelengths (energies) and computed electronic values, such as absorption wavelengths (λ), excitation energies (E), oscillator strengths (f), and major contributions of the transitions and assignments of electronic transitions are tabulated in Table 4. Calculations of the molecular orbital geometry show that the visible absorption maxima of this molecule

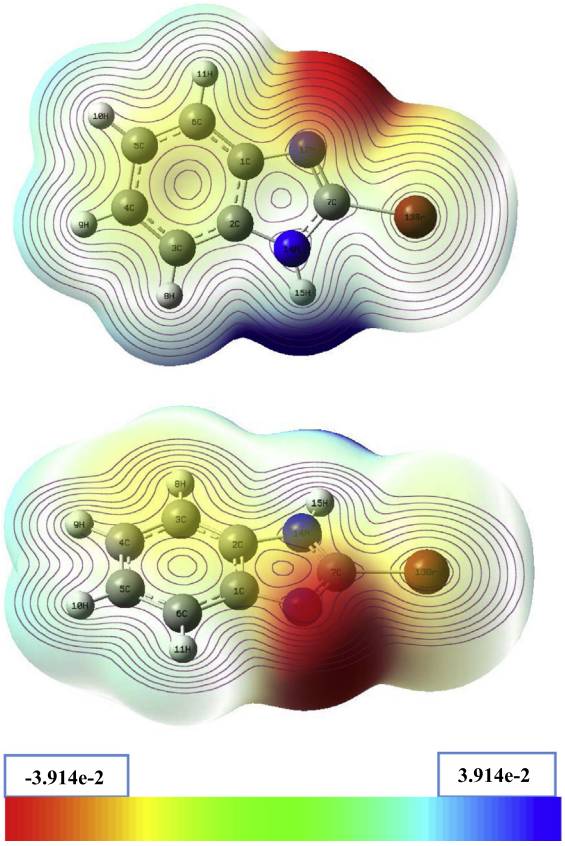

Fig. 11. MEP map for 2Br1HB molecule.

correspond to the electron transition between frontier orbitals such as transition from HOMO to LUMO. As can be seen from Table 4, the calculated absorption maxima values were found to be 252.62, 243.88, 239.45 nm in ethanol solution and 252.79, 243.73, 239.63 nm in DMSO and 252.50, 243.61, 239.32 in water at DFT/B3LYP/6-311+G(d,p) method. The predicted absorption maxima values in gas phase were found to be 251.11, 248.35, 235.01 nm, these excitations correspond to π - π^* transitions, which is in good agreement with the calculated maxima values in ethanol, DMSO and water, respectively.

Frontier molecular orbital analysis

The most important orbitals in a molecule are the frontier molecular orbitals (FMOs), called highest occupied molecular orbital (HOMO) and lowest unoccupied molecular orbital (LUMO). They are very useful to physicists and chemists. The HOMO energy characterizes the ability of electron giving; the LUMO characterizes the ability of electron accepting. While the energy of the HOMO is directly related to the ionization potential, LUMO energy is directly related to the electron affinity. Surfaces for the frontier orbitals are drawn to understand the bonding scheme of the present compound. Here, four important MOs were examined: the second highest and highest occupied MOs and the lowest and the second lowest unoccupied MOs are denoted as HOMO − 1, HOMO, LUMO and LUMO + 1, respectively. The plots of highest occupied molecular orbitals (HOMOs) and lowest unoccupied molecular orbitals (LUMOs) are shown in Fig. 7. In order to evaluate the energetic behavior of the title compound, we carried out calculations in DMSO, water, ethanol and gas phase. The energies of four important molecular orbitals of 2Br1HB: HOMO and HOMO − 1, LUMO and LUMO + 1 were calculated using B3LYP/6-311+G(d,p) and are presented in Table 5. It is clear from the figure that both HOMO and LUMO are located over the benzimidazole ring. The calculated energy values of the HOMO are −6.57, −6.66, −6.66 and −6.65 eV in gas, DMSO, water and ethanol, respectively. Similarly, the LUMO energy values are −1.02, −1.09, −1.09, −1.09 eV. The energy gap between HOMO and LUMO indicates the molecular chemical stability. In this molecule, the value of energy separation between the HOMO and LUMO are 5.55, 5.57, 5.57 and 5.56 eV in gas phase, DMSO, water and ethanol, respectively.

By using HOMO and LUMO energy values for a molecule, the global chemical reactivity descriptors of molecules such as chemical hardness (η), chemical potential (μ), softness (S), electronegativity (χ) and electrophilicity index (ω) were defined [50,51]. On the basis of E_{HOMO} and E_{LUMO}, these are calculated using the below equations. Using Koopman's theorem [52] for closed-shell molecules,

The hardness of the molecule is

$$\eta = (I - A)/2 \tag{5}$$

The chemical potential of the molecule is

$$\mu = -(I + A)/2 \tag{6}$$

The electronegativity of the molecule is

$$\chi = (I + A)/2 \tag{7}$$

The electrophilicity index of the molecule is

$$\omega = \mu^2/2\eta \tag{8}$$

where A is the ionization potential and I is the electron affinity of the molecule. I and A can be expressed through HOMO and LUMO orbital energies as $I = -E_{HOMO}$ and $A = -E_{LUMO}$. The calculated values of hardness, electronegativity, chemical potential, and electrophilicity index of our molecule in gas phase are 2.77, 3.79, −3.79 and 2.59, respectively. Similarly these values calculated by DFT method in three different solutions are listed in Table 5.

Total, partial, and overlap population density-of-states

In the boundary region, neighboring orbitals may show quasi degenerate energy levels. In such cases, consideration of only the HOMO and LUMO may not yield a realistic description of the frontier orbitals. For this reason, the TDOS, PDOS, and OPDOS or COOP (Crystal Orbital Overlap Population) density of states [53–55], in terms of Mulliken population analysis were calculated and created by convoluting the molecular orbital information with Gaussian curves of unit height and FWHM of 0.3 eV by using the GaussSum 2.2 program [24]. The TDOS, PDOS and OPDOS of 2Br1HB are plotted in Figs. 8–10, respectively. The OPDOS shows the bonding, anti-bonding and nonbonding nature of the interaction of the two orbitals, atoms or groups. A positive value of the OPDOS indicates a bonding interaction (because of the positive overlap population), negative value means that there is an anti-bonding interaction (due to negative overlap population) and zero value indicates nonbonding interactions [56]. Additionally, the OPDOS diagram allows us to the determine and compare the donor–acceptor properties of the ligands and ascertain the bonding and non-bonding. In the boundary region, neighboring orbitals may show quasi degenerate energy levels. Thus the OPDOS diagram is shown in Fig. 10, and some of the orbitals of energy values of interaction between selected groups which are shown from figures easily, phenyl group ↔ nitrogen atom (blue line) system are negative, that is anti-bonding interaction as well as nitrogen ↔ bromine atom (light green line). As can be seen from the OPDOS plots for 2Br1HB have bonding and anti-bonding character in frontier HOMO and LUMO molecular orbitals for phenyl ring and nitrogen atoms.

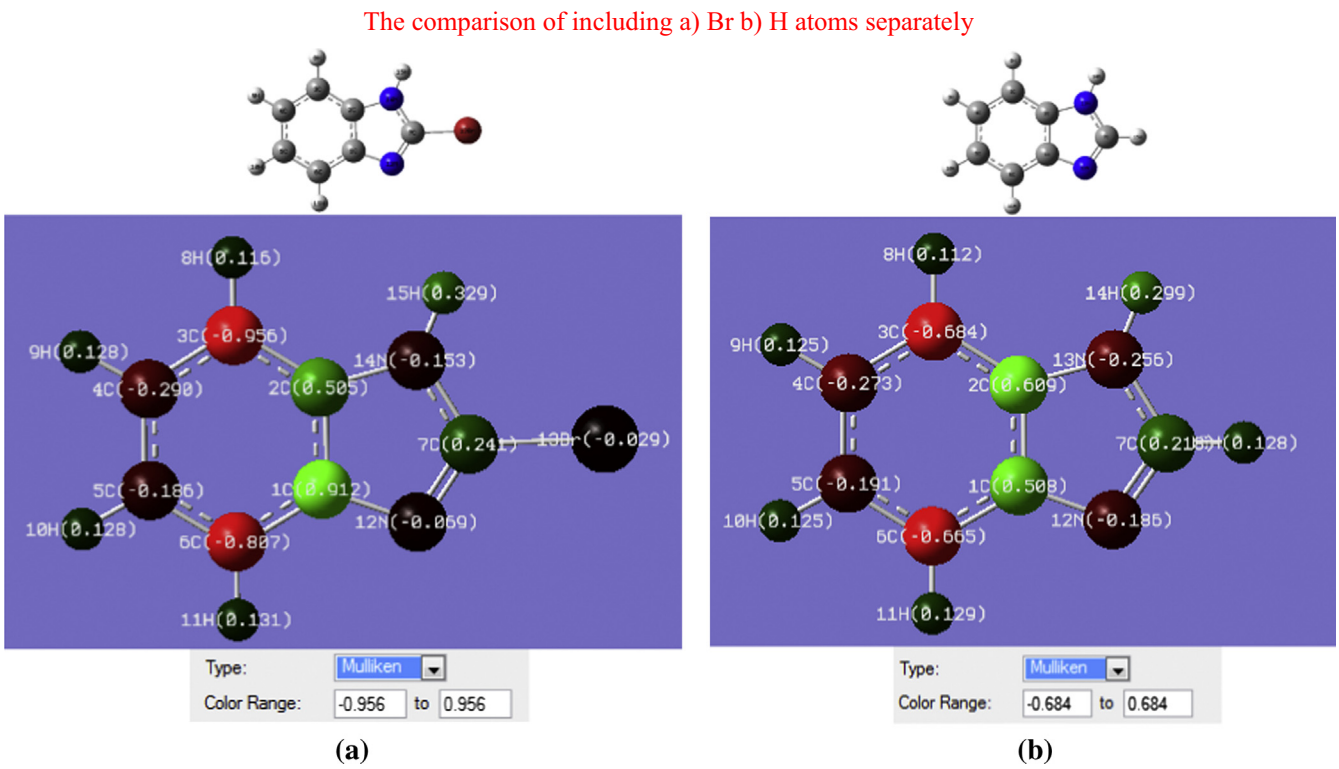

Fig. 12. The Mulliken charge distribution for (a) 2Br1HB and (b) benzimidazole.

Table 6
Comparison of Mulliken charges of 2Br1HB using by B3LYP/6-311+G(d,p) basis set.

Atoms	2Br1HB	Benzimidazole
C1	0.912	0.515
C2	0.505	0.616
C3	−0.956	−0.687
C4	−0.290	−0.274
C5	−0.186	−0.189
C6	−0.807	−0.680
C7	0.241	0.230
H8	0.116	0.113
H9	0.128	0.125
H10	0.128	0.125
H11	0.131	0.129
N12	−0.069	−0.186
Br13	−0.029	–
N14	−0.153	−0.261
H15	0.329	0.301
H	–	0.123

Table 7
Thermodynamic properties at different temperatures at the B3LYP/6-311+G(d,p) for 2Br1HB.

T (K)	C (cal mol^{-1} K^{-1})	S (cal mol^{-1} K^{-1})	ΔH (kcal mol^{-1})
100	11.123	66.175	0.978
150	15.438	72.294	1.740
200	20.074	77.935	2.726
250	24.889	83.374	3.949
298.15	29.511	88.504	5.354
300	29.686	88.700	5.413
350	34.280	93.931	7.113
400	38.543	99.056	9.034
450	42.411	104.057	11.159
500	45.875	108.917	13.467
550	48.956	113.627	15.939
600	51.691	118.179	18.556
650	54.122	122.573	21.302
700	56.290	126.812	24.162

Molecular electrostatic potential

MEP provides a visual method to understand the relative polarity of the molecule. To predict reactive sites for electrophilic and nucleophilic attack of the investigated molecule, MEP studies were carried out by B3LYP using 6-311+G(d,p) basis set. A visual representation of the chemically active such as the negative (red) regions of the MEP are related to electrophilic reactivity and the positive (blue) regions to nucleophilic reactivity, as shown in Fig. 11. Potential increases in the order red < orange < yellow < green < blue. The color code of these maps is between −3.914 e^{-2} (deepest red) and 3.914 e^{-2} (deepest blue) in the compound, where blue indicates the strongest attraction and red indicates the strongest repulsion. As can be seen from the MEP map of the title molecule, while regions having the negative potential are over the electronegative atom (oxygen atom) and nitrogen atom, the regions having the positive potential are over the hydrogen atoms.

Mulliken atomic charges

It is clear that Mulliken populations yield one of the simplest pictures of charge distribution and Mulliken charges render net atomic populations in the molecule. The charge distributions of 2Br1HB and benzimidazole were calculated by B3LYP/6-311+G(d,p) level of theory and shown in Fig. 12a and b. Comparison of Mulliken charges of 2Br1HB and benzimidazole is presented in Table 6. In all these compounds among the ring carbon atoms C1/C2/C7 have positive charges 0.912e/0.505e/0.241e for 2Br1HB and 0.515e/0.616e/0.230e for benzimidazole while others have negative charges. In case of 2Br1HB, it may be the reason of the substitution of electronegative nitrogen atoms on C1/C2 atoms and Br atom on C7 respectively. In case of benzimidazole C7 atom has less positive charge when compared to C7 atom of 2Br1HB. The C3 atom of the phenyl ring of 2Br1HB has the highest negative charge when compared to other carbon atoms. Similar situation is also observed in case of benzimidazole. N14 nitrogen atom has

the high negative charge (−0.153e) while the other nitrogen atom has less negative charge (−0.069e) for 2Br1HB. H15 atom of 2Br1HB has the high positive charge (0.329e). This may be due to N—H···N intermolecular interaction. Similar results are also found in benzimidazole. The comparison of the Mulliken charge distribution histogram for 2Br1HB and benzimidazole is shown in Fig. S3.

Thermodynamic properties

The thermodynamic functions viz, heat capacity at constant pressure (C), entropy (S) and enthalpy changes (ΔH) for the title compound were evaluated from the theoretical harmonic frequencies obtained from B3LYP/6-311+G(d,p) method in the temperature range of 100–700 K and are listed in Table 7. It can be observed that these thermodynamic parameters increase with the rise of temperature due to the fact that the molecular vibrational intensities increase with temperature [57]. The correlation equations between heat capacity, entropy, enthalpy changes and temperatures are fitted by quadratic formula. The correlation graphics of temperature dependence of thermodynamic functions for 2Br1HB molecule are shown in Fig. S4.

Conclusion

The spectroscopic properties such as molecular parameters, frequency assignments, and electronic transitions of 2Br1HB by using FT-IR, FT-Raman, dispersive Raman, ^{1}H and ^{13}C NMR techniques were analyzed both experimentally and theoretically. Theoretical UV–Vis analysis, HOMO and LUMO energy of 2Br1HB in the ground state were calculated by using DFT. The theoretical support was addressed by the example of DFT/B3LYP/6-311+G(d,p) calculations, and the peculiarities and limitations of the theoretical approach to the analysis were considered. On the basis of the experimental results and PED calculations, assignments of all fundamental vibrational frequencies were done. A good correlation between the observed and scaled wavenumbers was obtained for the title compound. The contributions of molecule orbitals were analyzed by using the TDOS, PDOS, and OPDOS density of states. Thermodynamic properties in the range from 100 to 700 K were obtained. The molecular orbitals, MEP contour/surface and NBO analysis may lead to the understanding of properties and activity of 2Br1HB and may also aid the use of 2Br1HB in various advanced pharmaceutical applications.

Appendix A. Supplementary data

Supplementary data associated with this article can be found, in the online version, at http://dx.doi.org/10.1016/j.molstruc.2014.10.025.

References

[1] J.B. Foresman, A. Frisch, Exploring Chemistry with Electronic Structure Methods, second ed., Gaussian Inc., Pittsburgh, 1996.
[2] W. Koch, M.C. Holthausen, A Chemist's Guide to Density Functional Theory, Wiley VCH, 2000.
[3] W. Nawrocka, M. Zimecki, T. Kuznicki, Arch. Pharm. 332 (1999) 85.
[4] A. De Dios, C.H. Shih, B.L. De Uralde, J. Med. Chem. 48 (2005) 2270.
[5] V. Rajendiran, M. Murali, E. Suresh, S. Sinha, K. Somasundaram, M. Palaniandavar, Dalton Trans. (2008) 148.
[6] J.B. Camden, US Patent 6,077,862, 2002.
[7] P.K. Naithani, V.K. Srivastava, A.K. Saxena, J.P. Barthwal, T.K. Gupta, K. Shanker, Indian J. Exp. Biol. 28 (12) (1990) 1145.
[8] N.M. Goudgaon, V. Dhondiba, A. Vijayalaxmi, Indian J. Heterocycl. Chem. 13 (2004) 271.
[9] D. Sperandio, A.R. Gangloff, J. Litvak, R. Goldsmith, J.M. Hataye, V.R. Wang, E.J. Shelton, K. Elrod, J.W. Janc, J.M. Clark, K. Rice, S. Weinheimer, K.S. Yeung, N.A. Meanwell, D. Hernandez, A.J. Staab, B.L. Venables, J.R. Spencer, Bioorg. Med. Chem. Lett. 12 (2002) 3129.
[10] Fabio da Silva Miranda, Fabrício Gava Menezes, Juliano Vicente, Adailton J. Bortoluzzi, César Zucco, Ademir Neves, Norberto Sanches Gonçalves, J. Mol. Struct. 938 (2009) 1.
[11] Nour T. Abdel-Ghani, Maha F. Abo El-Ghar, Ahmed M. Mansour, Spectrochim. Acta A 104 (2013) 134.
[12] S. Sudha, M. Karabacak, M. Kurt, M. Cinar, N. Sundaraganesan, Spectrochim. Acta A 84 (2011) 184.
[13] L. Sinha, O. Prasad, M. Karabacak, H.N. Mishra, V. Narayan, A.M. Asiri, Spectrochim. Acta A 120 (2014) 126.
[14] M. Kurt, P. Chinna Babu, N. Sundaraganesan, M. Cinar, M. Karabacak, Spectrochim. Acta A: Mol. Biomol. Spect. 79 (2011) 1162–1170.
[15] M.J. Frisch et al., Gaussian 09, Revision A.1, Gaussian Inc., Wallingford CT, 2009.
[16] P. Hohenberg, W. Kohn, Phys. Rev. 136 (1964) B864.
[17] A.D. Becke, J. Chem. Phys. 98 (1993) 5648.
[18] C. Lee, W. Yang, R.G. Parr, Phys. Rev. B 37 (1988) 785.
[19] E. Frisch, H.P. Hratchian, R.D. Dennington II, T.A. Keith, John Millam, B. Nielsen, A.J. Holder, J. Hiscocks. Gaussian, Inc., GaussView Version 5.0.8, 2009.
[20] M.H. Jamroz, Vibrational Energy Distribution Analysis: VEDA 4 Program, Warsaw, Poland, 2004.
[21] E.D. Glendening, C.R. Landis, F. Weinhold, Comput. Mol. Sci. (2011) 1–42 (John Wiley & Sons, Ltd. WIREs).
[22] R. Ditchfield, J. Chem. Phys. 56 (1972) 5688.
[23] K. Wolinski, J.F. Hinton, P. Pulay, J. Am. Chem. Soc. 112 (1990) 8251.
[24] N.M. O'Boyle, A.L. Tenderholt, K.M. Langner, J. Comp. Chem. 29 (2008) 839.
[25] S. Shen, G.A. Guirgis, J.R. Durig, Struct. Chem. 12 (2001) 33.
[26] D. Michalska, R. Wysokinski, Chem. Phys. Lett. 403 (2005) 211.
[27] D. Michalska, RAINT, a Computer Program for Calculation of Raman Intensities from the Gaussian Outputs, Wrocław University of Technology, 2002.
[28] Long-Huai Cheng, Zheng Zheng, Zhi-Li Han, Zhi-Chao Wu, Hong-Ping Zhou, Acta Cryst. E68 (2012) o2890. ISSN 1600.
[29] R.I. Castillo, L.A. Rivera Montalvo, S.P. Hernandez Rivera, J. Mol. Struct. 877 (2008) 10.
[30] M. Arivazhagan, D. Anitha Rexalin, Spectrochim. Acta Part A 83 (2011) 553.
[31] M. Arivazhagan, R. Meenakshi, Spectrochim. Acta Part A 91 (2012) 419.
[32] J.P. Merrick, D. Moran, L. Radom, J. Phys. Chem. A 111 (2007) 11683.
[33] L. Ushakumari, H.T. Varghese, C.Y. Panicker, T. Ertan, I. Yildiz, J. Raman Spectrosc. 39 (2008) 1832.
[34] J. Coates, R.A. Meyers, Introduction to Infrared Spectrum, A Practical Approach, John Wiley and Sons Ltd, Chichester, 2000.
[35] M. Karabacak, M. Kurt, A. Atac, J. Phys. Org. Chem. 22 (2009) 321–330.
[36] N. Sundaraganesan, H. Saleem, S. Mohan, Spectrochim. Acta 59A (2003) 2511.
[37] G. Thilagavathi, M. Arivazhagan, Spectrochim. Acta 79A (2010) 389.
[38] M. Govindarajan, K. Ganasan, S. Periandy, M. Karabacak, Spectrochim. Acta A 79 (2011) 646–653.
[39] R. Shanmugam, D. Sathyanarayana, Spectrochim. Acta 40A (1984) 757.
[40] M. Govindarajan, M. Karabacak, A. Suvitha, S. Periandy, Spectrochim. Acta A 89 (2012) 137–148.
[41] G. Varsanyi, Assignments of Vibrational Spectra of Seven Hundred Benzene Derivatives, vol. 1–2, Adam Hilger, 1974.
[42] A. Fu, D. Du, Z. Zhou, Spectrochim. Acta 59 (2003) 245.
[43] M. Karabacak, E. Sahin, M. Cinar, I. Erol, M. Kurt, J. Mol. Struct. 886 (2008) 148.
[44] N. Sundaraganesan, S. Ilakiamani, P. Subramani, B.D. Joshua, Spectrochim. Acta 67A (2007) 628.
[45] L.J. Bellamy, The IR Spectra of Complex Molecules, John Wiley and Sons, New York, 1975.
[46] A. Spire, M. Barthes, H. Kallouai, G. De Nunzio, Physics D 137 (2000) 392.
[47] C.Y. Panicker, H.T. Varghese, T. Tansani, Turk. J. Chem. 33 (2009) 1.
[48] C. James, A. AmalRaj, R. Reghunathan, I. Hubert Joe, V.S. JayaKumar, J. Raman Spectrosc. 37 (2006) 1381.
[49] H.O. Kalinowski, S. Berger, S. Braun, Carbon-13 NMR Spectroscopy, John Wiley & Sons, Chichester, 1988.
[50] R. Parr, L. Szentpaly, S. Liu, Am. Chem. Soc. 121 (1999) 1922.
[51] P. Chattraj, B. Maiti, U. Sarkar, J. Phys. Chem. A107 (2003) 4973.
[52] T.A. Koopmans, Physica 1 (1934) 104.
[53] R. Hoffmann, Solids and Surfaces: A Chemist's View of Bonding in Extended Structures, VCH Publishers, New York, 1988.
[54] T. Hughbanks, R. Hoffmann, J. Am. Chem. Soc. 105 (1983) 3528.
[55] J.G. Małecki, Polyhedron 29 (2010) 1973.
[56] M. Chen, U.V. Waghmare, C.M. Friend, E. Kaxiras, J. Chem. Phys. 109 (1998) 6680–6854.
[57] J.B. Ott, J. Boerio-Goates, Chemical Thermodynamics: Advanced Applications, Calculations from Statistical Thermodynamics, Academic Press, 2000.